Cationic polymer effect on brown adipogenic induction of dedifferentiated fat cells

Aslı Sena Karanfil [a], Fiona Louis [b,**], Yoshihiro Sowa [c,d,e], Michiya Matsusaki [a,b,*]

[a] *Department of Applied Chemistry, Graduate School of Osaka University, Japan*
[b] *Joint Research Laboratory (TOPPAN) for Advanced Cell Regulatory Chemistry, Graduate School of Osaka University, Japan*
[c] *Department of Plastic Surgery, Jichi Medical University, Shimotsuke, Tochigi, Japan*
[d] *Department of Plastic and Reconstructive Surgery, Graduate School of Medical Sciences, Kyoto Prefectural University of Medicine, Japan*
[e] *Department of Plastic and Reconstructive Surgery, Graduate School of Medicine, Kyoto University, Japan*

ABSTRACT

Obesity and its associated comorbidities place a substantial burden on public health. Given the considerable potential of brown adipose tissue in addressing metabolic disorders that contribute to dysregulation of the body's energy balance, this area is an intriguing avenue for research. This study aimed to assess the impact of various polymers, including collagen type I, fibronectin, laminin, gelatin, gellan gum, and poly-L-lysine (PLL), on the *in vitro* brown adipogenic differentiation of dedifferentiated fat cells within a fibrin gel matrix. The findings, obtained through RT-qPCR, immunofluorescent imaging, ELISA assay, and mitochondria assessment, revealed that PLL exhibited a significant browning-inducing effect. Compared to fibrin-only brown-like drops after two weeks of incubation in brown adipogenic medium, PLL showed 6 ($\pm$3) times higher UCP1 gene expression, 5 ($\pm$2) times higher UCP1 concentration by ELISA assay, and 2 ($\pm$1) times higher mitochondrial content. This effect can be attributed to PLL's electrostatic properties, which potentially facilitate the cellular uptake of crucial brown adipogenic inducers such as the thyroid hormone, triiodothyronine (T3), and insulin from the induction medium.

1. Introduction

Obesity, marked by an excessive accumulation of body fat, is a complex and far-reaching global health issue [1]. It is a significant risk factor for a range of serious diseases including, but not limited to, type 2 diabetes [2], high blood pressure [3], heart disease [4], stroke [5], certain cancers [6], musculoskeletal problems [7], and respiratory issues [8]. According to the 2023 World Obesity Atlas, obesity is anticipated to affect nearly two billion individuals globally by 2035 [9].

The increasing prevalence of global obesity has highlighted the importance of studying adipose tissue and its related metabolic complexities. Among mammals, adipose tissue is mainly classified into two types: white adipose tissue (WAT), responsible for storing energy as intracellular triglycerides and secreting hormones, and brown adipose tissue (BAT), involved in regulating body temperature through non-shivering thermogenesis [10]. Additional adipose tissue types such as beige/bright [11], pink [12], and yellow [13] have also been

documented in scientific literature [14]. Brown adipocytes facilitate heat dissipation by uncoupling proton transport from ATP synthesis. Due to their abundant mitochondria and the presence of "uncoupling protein 1" (UCP1) [15], BAT can convert electrochemical energy generated during respiration into heat by uncoupling of lipid oxidation from ATP generation in mitochondria [16,17]. This metabolic process contributes to oxygen uptake, caloric consumption, and body temperature regulation [17]. Because BAT strongly impacts calorie expenditure, it is considered a potential therapeutic target in combating obesity.

White adipocytes exhibit high plasticity and high reprogramming capacity. *In vitro*, mature adipocytes can undergo reprogramming, transitioning into dedifferentiated fat cells (DFAT cells), recognized as a novel form of stem cell [18]. Once adhered in fully medium-filled cell culture flasks, white adipocytes shed their cytoplasmic lipid content, evolving into DFAT cells within approximately one week [19]. Through this process, they acquire multipotent characteristics similar to mesenchymal stem cells (MSC), expressing MSC-related markers such as CD44,

CD90, CD73, and CD105 [20], displaying substantial redifferentiation potential across osteogenic [21,22], chondrogenic [23], and adipogenic [24] lineages. This exceptional capacity for redifferentiation, combined with a straightforward isolation process [18,25], establishes DFATs as a valuable and abundant resource applicable in tissue engineering, regenerative medicine, cell therapy, and stem cell research. As detailed in our previous study [26], DFATs offer important advantages, such as their relatively easy and abundant acquisition from waste adipose tissues obtained through procedures like liposuction, compared to adipose-derived stem-cells (ADSCs), in tissue engineering studies.

Given its critical role, the engineering of adipose tissue represents a promising avenue for assessing and enhancing endocrine metabolism within the body [27–29]. Various scaffold materials have been explored to emulate the native tissue environment and bolster adipose tissue biological functions, but there has been less research conducted on thermogenic adipose tissue engineering as a therapeutic approach for obesity-related diseases [30]. The materials used in these few studies have been a range of natural and synthetic options such as collagen type I [31], hyaluronic acid [32], gelatin [33], and polyethylene glycol (PEG) derivatives [34,35].

In this study, we chose fibrin gel for the basic material to construct our tissues. It is a well-regarded option in tissue engineering research owing to its biocompatibility, biodegradability, and non-toxic nature. Typically serving as a matrix or carrier for cells in adipose tissue engineering studies [36,37], it is commonly used as a matrix or cell carrier. Used by themselves, standalone fibrin gels have a limited impact on adipogenesis [36], and their dehydration and degradation in extended culture conditions restrict their utility. Nevertheless, they do offer mechanically conducive environmental conditions for soft tissue engineering applications. When combined with collagen microfibers (CMF), this gel facilitates the regeneration of the structure of adipose tissue before implantation, employing white adipocytes, resulting in notably high cell viability [37]. However, a review of the relevant literature on *in vitro* brown adipose tissue engineering was unable to identify any study reporting the effect of a fibrin matrix mixed with different polymers on brown adipogenic differentiation.

We therefore generated brown-like adipose tissue drops by encapsulating DFATs derived from human white adipocytes within fibrin gel mixed with various biopolymers, including collagen type I, collagen type IV, fibronectin, laminin, gelatin, gellan gum (GG), and poly-L-lysine (PLL) as a cationic polymer. We investigated the impact of polymer supplementation on browning through lipid droplet size analysis, mitochondrial assessment, oxygen consumption rates and PCR analysis within the developed drops. This proposed research could have a profound impact, providing potential applications for PLL in the field of thermogenic adipose tissue engineering to address obesity and related comorbidities.

2. Materials and methods

2.1. Chemicals and reagents

Fibrinogen (from bovine plasma, F8630), Thrombin (from bovine plasma, T4648), Fibronectin (from human plasma, F2006), Collagen type IV (from human placenta, C7521), Poly-L-lysine (PLL, P4707), Poly-L-lysine FITC conjugated (P3543), Phosphate buffered saline powder (PBS, D5652), Collagenase from *Clostridium histolyticum* (Type I, C0130) and Triton-X 100 (T8787), Bovine Serum Albumin (BSA, 3294), Dexamethasone (D4902), Indomethacin (I7378) 3-Isobutyl-1-methylxanthine (IBMX, I5879), Insulin (I6634) Rosiglitazone (R2408), 3,3′,5-Triiodo-L-thyronine sodium salt (T3, T6397), Hoechst 33,324 (H3570) were purchased from Sigma-Aldrich (St Louis, MO, USA). Trypan Blue (T10282), MitoTracker™ Deep Red FM (M7212), UCP1 polyclonal antibody (PA1-24894), Qubit HS DNA Assay Kit (Q3285), Anti-rabbit secondary antibody Alexa Fluor® 647, Nile Red (N1142), PicoPure™ RNA Isolation kit (KIT0204) Penicillin, Streptomycin were obtained

from Thermo Fisher Scientific (Whaltam, MA, USA). Gelatin (077–03155), 4%-paraformaldehyde (16,310,245), Na$_2$SO$_3$ (198–03412), Trypsin (207,192–83) were purchased from Wako Pure Chemical Industries (Tokyo, Japan). Collagen type I FAM conjugated (AS-85111) obtained from Funakoshi (Tokyo, Japan). Anti Heperan Sulphate (370255-S) was purchased from AMS Biotechnology (Abingdon, UK). Dulbecco's Modified Eagle Medium (DMEM) high glucose (08458–16) was came from Nacalai Tesque Inc. (Kyoto, Japan). Anti-mouse Heparan Sulphate antibody (370255-S) purchased from AMS Biotechnology (Europe) Limited, Abingdon, UK. Human UCP1 ELISA Kit (MBS451508) was purchased from MyBioSource (San Diego, USA). Oxoplate 96-well round-bottomed OxoPlate (OP96U) was came from PreSens Precision Sensing, (Regensburg, Germany). Live/Dead® viability assay kit (PK-CA707-30002) purchased from PromoKine (Heidelberg, Germany). Phosphate Buffer Saline (PBS, 14,249–24) was came from Nacalai Tesque Inc. (Kyoto, Japan). Fetal Bovine Serum (FBS, 10,270,106) was obtained from Gibco. Adipocyte Differentiation medium (811D-250) was came from Cell Applications Inc. (San Diego, USA). Collagen type I (from bovine dermis, Atelocell, IPC-50) was purchased from Koken (Tokyo, Japan). Laminin (354,259) was obtained from Corning (Arizona, USA). Gellan Gum (8H1121A) was came from Sansho (Osaka, Japan). Phalloidin-iFluor 594 Reagent (ab176757 purchased from Abcam (Cambridge, UK). RNase-free DNase set (79,254) was purchased from Qiagen (Hilden, Germany). iScript™ cDNA Synthesis Kit, Bio-Rad (California, USA). TaqMan gene expression assays (Applied Biosystems) was purchased from Thermo Fisher Scientific (Whaltam, MA, USA).

2.2. Cell culture experiments

2.2.1. Obtaining of DFATs

DFATs were obtained using our previously reported method [26]. Human adipose tissues were obtained from patients at Kyoto University Hospital, then mature adipocytes were freshly isolated. Briefly, tissues were washed with phosphate-buffered saline (PBS) with 5 % penicillin-streptomycin. Adipose tissue as 2–3 g per well of a 6-well plate, was minced, and a collagenase solution (2 mg/mL in Dulbecco's modified Eagle Medium (DMEM) with 5 % bovine serum albumin (BSA) and 1 % penicillin-streptomycin) was added for 1 h at 37 °C with 250 rpm rotation. After filtration and centrifugation, mature adipocytes were collected from the top layer, and stromal vascular fraction from the bottom. After discarding the in-between liquid, washing was performed with PBS with 5 % BSA, 1 % penicillin-streptomycin and a final wash in DMEM with 10 % fetal bovine serum (FBS) and 1 % penicillin-streptomycin. Then, freshly isolated mature adipocytes were cultured at a seeding density of 5.0×10^4/cm^2 in polystyrene flasks fully filled with DMEM containing 20 % FBS and 1 % penicillin-streptomycin. The flasks were securely capped to prevent medium leakage and incubated at 37 °C for one week. After incubation, the medium was aspirated, and the resulting DFATs were detached through trypsinization (Trypsin-EDTA 0.25 %). These obtained DFATs (passage numbers 4 to 7) were used in subsequent experiments.

3. Ethics statement

The adipose tissues were collected from Kyoto University Hospital (Kyoto, Japan) after abdominal adipose tissue or liposuction isolation of three human donors aged 41, 45, and 53 years old, with a BMI of 22.40, 25.78, and 20.46, respectively. All use was approved by the Osaka University Research Ethics Review Committee (approval number: L026).

3.1. BAT drops seeding

The graphical overview of the sample preparation is shown in Fig. 1. DFATs were mixed at a seeding density of 4.0×10^6 cells/mL with a
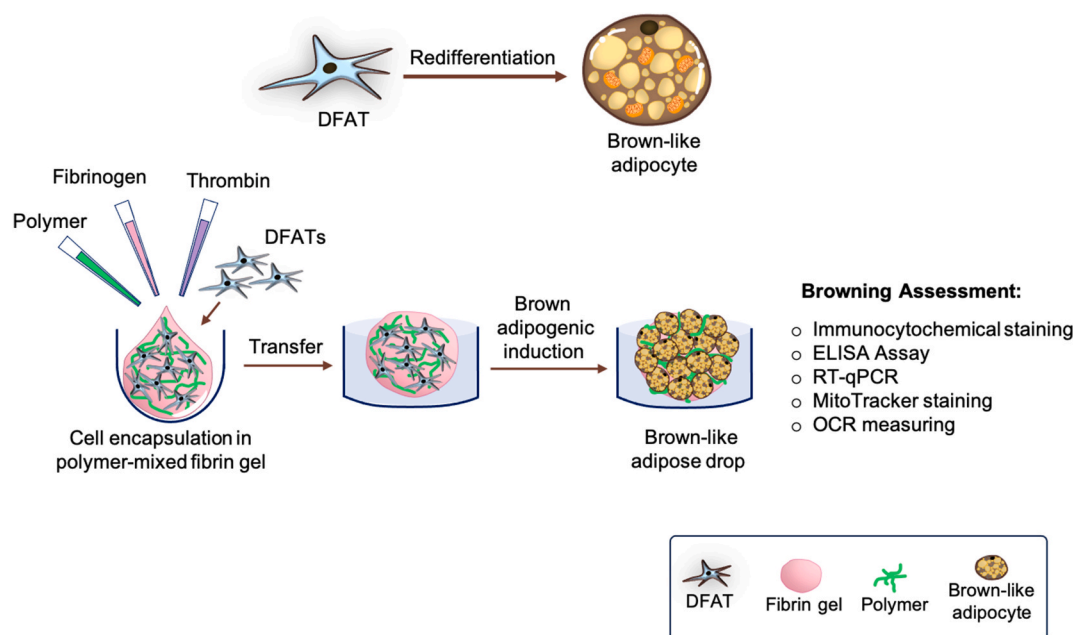
Fig. 1. Schematic overview of the research design. DFATs were encapsulated within a fibrin gel by using a round bottom 96 well plate with variety of polymers, then samples transferred into ultra-low attachment 24 well plate and cultured in brown adipogenic induction medium for 2 weeks. Mixed polymers are collagen I, collagen IV, fibronectin, laminin, gelatin, and gellan gum, and PLL.

fibrinogen solution (final concentration of 6 mg/mL from a stock solution (50 mg/mL) in DMEM 0 % FBS, 1 % penicillin-streptomycin, filtered using a 0.2 μm filter) and a thrombin solution (final concentration of 3 U/mL from a stock solution (10 U/mL) in DMEM, 10 % FBS, 1 % penicillin-streptomycin, filtered using a 0.2 μm filter). The resulting mixture was directly seeded to a 96-well ultra-low attachment round-bottomed plate at a volume of 5 μL using wide pipette tips and incubated at 37 °C for 20 min for gelation. Subsequently, after adding 80 μL of growth medium (GM, 10 % FBS, 1 % penicillin-streptomycin in high-glucose DMEM) to detach drops, samples were transferred to a 24-well ultra-low attachment plate and incubated in 500 μL of GM in each well for 2 days. The culture medium was then fully replaced with brown adipogenic differentiation medium (BAM), containing 0.5 μM dexamethasone, 125 nM indomethacin, 250 μM IBMX, 850 nM bovine insulin, 1 μM rosiglitazone, 120 nM triiodothyronine (T3), 1 % penicillin-streptomycin, and 10 % FBS in high-glucose DMEM [34]. For polymer-mixed drops, all polymers (collagen type I, fibronectin, laminin, collagen type IV, gelatin, GG) were first dissolved in PBS (pH 7.4), filtered through a 0.2 μm filter, and then mixed with the cell-fibrin gel mixture at a final concentration of 50 μg/mL, except for PLL. For PLL-mixed drops, the polymer was mixed at concentrations of 5, 10, or 20 μg/mL. Samples were cultured in BAM for 2 weeks, with half the medium replaced every two days throughout the culturing period. To obtain WAT drops, samples were cultured in Adipocyte Differentiation Medium (Cell Applications Inc.) for 2 weeks with half the medium replaced every two days throughout the culturing period. For undifferentiated DFAT drops in fibrin gel, samples were cultured in GM for the same duration with half the medium replaced every two days.

3.2. Immunofluorescence imaging

After the two-week incubation in BAM and WAM, the samples were washed three times with PBS, followed by fixation in a 4 % para-formaldehyde solution in PBS overnight at 4 °C. To enhance permeability, samples were treated with 0.05 % Triton X-100 in PBS for 15 min and then incubated for 1 h at room temperature in 1 % BSA in PBS to minimize nonspecific staining. The anti-UCP1 antibody, diluted in 1 % BSA (1:500 dilution), was applied to the samples overnight at 4 °C.

Subsequently, the samples were exposed to Alexa Fluor® 647 secondary antibodies (dilution 1:200) for 2 h at room temperature. Intracellular lipid accumulation was visualized using Nile Red (final concentration: 50 ng/mL), and nuclei were counterstained with Hoechst (final concentration: 10 ng/mL). For mitochondrial staining on days 7 and 14, samples were washed three times with PBS and incubated in Mito-Tracker dye diluted in medium (10 % FBS, 1 % penicillin-streptomycin in DMEM high glucose without phenol red) for 30 min at 37 °C in a 5 % CO_2 incubator. The samples were then washed with PBS. All samples were rinsed in PBS and examined using an FV3000 Confocal Laser Scanning Microscope (CLSM) (Olympus, Tokyo, Japan). To compare UCP1 content, lipid accumulation, and mitochondrial abundance, Z-stack images were captured using the same procedures, and maximum intensity projection was performed while maintaining consistent exposure time and excitation power for all samples. Data were acquired by measuring the total fluorescence intensity of UCP1, lipid droplets, and MitoTracker, normalized to the total fluorescent intensity of Hoechst for each drop, using Image J software (Fiji for Mac OS X). For the heparan sulphate staining on DFATs incubated in fluorescein isothiocyanate (FITC)-labeled PLL (final concentration: 10 μg/mL) including DMEM (10 % FBS, 1 % penicillin-streptomycin), cells were seeded on a 96-well plate with 10,000 DFATs per well. After 24 h incubation in GM at 37 °C in a 5 % CO_2 incubator, the medium was removed, FITC-PLL mixed in GM was inserted and the cells were incubated for 24 h. After fixation, permeabilization and blocking steps, the anti-heparan sulphate antibody, diluted in 1 % BSA (1:100 dilution) was applied to the samples overnight at 4 °C. The samples were then exposed to Alexa Fluor® 647 secondary antibodies (dilution 1:200) for 2 h at room temperature. Nuclei were counterstained with Hoechst (final concentration: 10 ng/mL). All samples were rinsed in PBS and then examined using an FV3000 CLSM (Olympus, Tokyo, Japan).

3.3. Lipid droplet size measurement

The samples incubated in BAM and white adipogenic medium (WAM) were subjected to intracellular lipid accumulation staining using Nile Red, with nuclei counterstained using Hoechst (see **2.3.** for details). Subsequently, the samples were rinsed in PBS and then examined on a

glass-bottomed surface dish using an FV3000 CLSM (Olympus, Tokyo, Japan) at a 60× magnification with immersion oil. Lipid droplet sizes were quantified using Image J (Fiji for Mac OS X), with 200 droplets measured for each image.

3.4. Cell viability assay

To assess the cell viability in PLL-mixed drops with different PLL concentrations (0, 10, 20 and 50 μg/mL), samples were cultured in GM overnight. Subsequently, a Live/Dead® viability assay kit was applied and compared with samples containing only fibrin. After three washes with PBS, cells were stained using Calcein, (final concentration: 2 μM/ green for living cells), and Ethidium Homodimer-1 (final concentration: 4 μM/red for dead cells) for 30 min at 37 °C in the dark, followed by imaging using an FV3000 CLSM (Olympus, Tokyo, Japan). The percentages of cell viability were quantified using Image J software on Z-stack images, captured with consistent laser power and step sizes for each.

3.5. RT-qPCR analysis

Gene expressions were assessed using real-time quantitative polymerase chain reaction (RT-qPCR). Total RNA from drops (6 drops combined per replicate) was isolated using a PicoPure™ RNA isolation kit according to the manufacturer's instructions. The extracted RNA was quantified using a Nanodrop™ N1000 device (Thermo Fisher Scientific, MA, USA). To convert the isolated RNA to DNA, an iScript cDNA synthesis kit was used as per the manufacturer's instructions. For DNA amplification, cDNA was amplified using Taqman Fast Advanced Mix with Taqman gene expression assays for UCP1, Cidea, PRDM16, and RPII (used as a housekeeping gene), following the manufacturer's protocol (Supplementary Table 1). The cDNA synthesis and RT-qPCR reactions were carried out using a StepOnePlus Real-Time PCR System (Thermo Fisher Scientific, MA, USA). RT-qPCR analysis was conducted on cells obtained from the three different donors, for a total number of replicates from 3 to 9.

3.6. UCP1 ELISA assay

Samples were washed three times with PBS and then treated with Trypsin-EDTA at 37 °C until the fibrin gel dissolved. The cells were collected by centrifugation, washed with cold PBS three times, and subjected to three cycles of freezing and thawing. After removing cellular debris through centrifugation at 1,500g, 4 °C for 10 min, a Human UCP1 ELISA Kit was used following the manufacturer's instructions. Data normalization was achieved by quantifying DNA using a Qubit HS DNA assay on the ELISA lysates.

3.7. Measurement of oxygen consumption rate

Polymer-mixed samples were washed three times with PBS, then transferred to a 96-well round-bottomed OxoPlate (OP96U, PreSens Precision Sensing). Four drops were added per well with DMEM containing 10 % FBS and 1 % penicillin-streptomycin, without phenol red. For plate calibration, eight wells were designated for 0 % O_2 standard (H_2O with 10 mg/mL sodium sulfite) and 100 % O_2 standard (respiration media), following the manufacturer's protocol. Oxygen concentrations were measured on day 14 and after an additional 24 h with the same plate using a plate reader equipped with two calibration standards and filter pairs for the indicator (excitation 540 nm, emission 650 nm) and reference (excitation 540 nm, emission 590 nm). Calibrations and oxygen levels were calculated following the manufacturer's manual, and the oxygen consumption rate in 24 h was determined. Data normalization was performed using DNA quantification with a Qubit HS DNA assay.

3.8. DNA quantification

A Qubit™ DNA HS Assay Kit was used with a Qubit™ 2.0 Fluorometer (Life Technologies, Thermo Fisher Scientific Inc.) for DNA quantification. Samples were washed with PBS and incubated in Trypsin-EDTA to dissolve the fibrin gel. They were then subjected to three cycles of freezing and thawing in Eppendorf tubes. The assay was performed following the manufacturer's instructions. For DNA normalization of the ELISA samples, the assay was performed directly on ELISA lysates.

3.9. Monitoring of T3 and insulin adsorption on PLL coated surfaces

The PLL coating was applied following the provider's protocol, involving a 5-min incubation at room temperature with the addition of 200 μL solution onto a 24-well polystyrene surface. Insulin and T3 solutions were prepared according to the provider's data sheet and added to the PLL-coated wells. Subsequently, samples were collected every 10 min, and the UV–Vis absorbances of samples with a final concentration of 1 μM for T3 and 10 μM for insulin were measured with a UV–Vis/NIR Spectrophotometer (V 670, Jasco Inc., Japan). The amount of adsorbed product on the surface over time was calculated using the obtained absorbance graphs (n = 3).

3.10. Zeta potential measurement

Zeta potential of insulin and T3 solutions were measured by a Malvern ZetaSizer. Solutions were prepared at the same concentration as for BAM, for T3 120 nM and insulin 850 nM. Then disposable folded capillary cells were filled with 800 μL of solutions and measurements were taken by dynamic light scattering at 25 °C (n = 3).

3.11. Statistical analysis

ANOVAs were performed using ezANOVA software to determine significant differences between pairs of data sets. Error bars represent standard deviation. p values < 0.05 were considered statistically significant.

4. Results

4.1. Brown adipogenic differentiation medium effect on browning

First, we confirmed the brown adipogenic induction potential of our culture conditions by comparing BAM and WAM in drop tissue formation. Lipid droplet size of differentiated brown and white adipocytes is well defined in the literature [38]. Therefore, we compared the effects of these two media on lipid droplet sizes. The lipid droplets of samples cultured in BAM and WAM for a duration of 14 days were stained with Nile Red, as illustrated in Fig. 2A. Notably, brown-differentiated cells exhibited significantly smaller ($p < 0.001$) lipid droplet diameters compared to their white-differentiated counterparts. The lipid droplet sizes of brown adipocytes were 2.4 (± 0.8) μm, whereas white-differentiated cells had larger droplets, measuring 7 (± 3) μm (Fig. 2B). This result confirms the morphological distinction between white and brown adipogenic differentiations. BAT is recognized for its elevated mitochondrial content. Consequently, mitochondrial content in both brown-differentiated and undifferentiated cells (BAM and GM respectively) was evaluated by quantification of mitochondrial abundance through MitoTracker staining, as illustrated in Fig. 2C. The results revealed a notably higher fluorescence intensity of mitochondria in brown-differentiated cells as opposed to undifferentiated cells, with a statistically significant difference ($p < 0.05$) indicating a substantial increase of 25 % (± 17).

Then, immunocytochemical visualization of the brown adipogenic marker UCP1 and lipid droplets was conducted on both brown
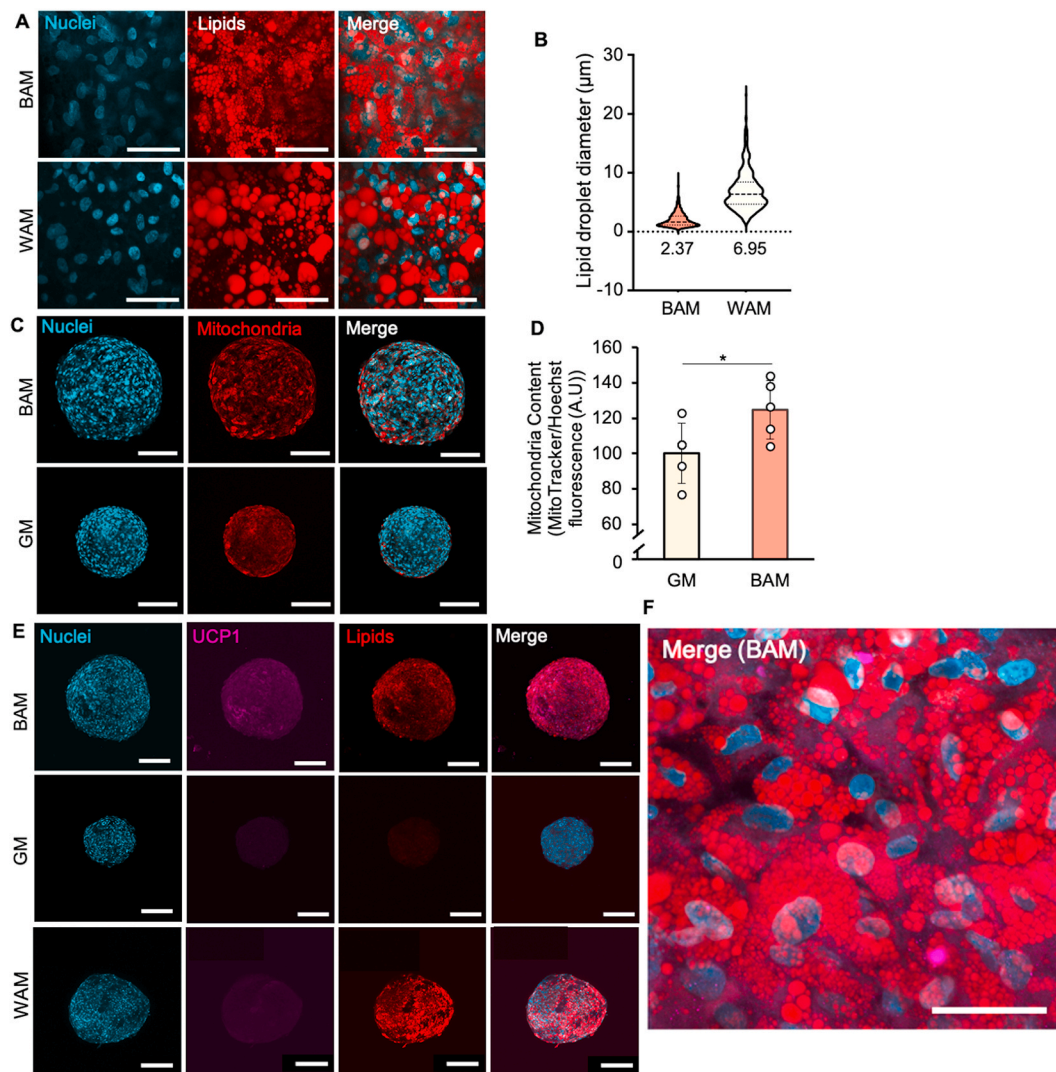
Fig. 2. Brown adipogenic differentiation medium (BAM) and growth medium (GM) effect assessment. A) Lipid droplets of differentiated cells were stained with Nile Red and Hoechst counterstaining was used to visualize nuclei (blue) (scale bar: 50 μm). B) Lipid droplet sizes of each drop were measured by Image J, with counted 200 lipid vesicle diameters of each drop (n = 3, three independent experiments from one donor). C) Representative MitoTracker staining images of mitochondria (red) and Hoechst counterstaining was used to visualize nuclei (blue) of fibrin only drops incubated in BAM and GM on day 14. Mitochondria and nuclei of cells are shown in Merge image (Scale bar: 200 μm). D) Measurement of the MitoTracker fluorescence of the drops incubated in BAM and GM, normalized by the either the DNA (Hoechst) fluorescence. Results are shown as mean ± standard deviation (n = 5, five independent experiments from one donor), * = $p < 0.05$. E) Representative images of immunocytochemical staining of Uncoupling protein 1 (UCP1, magenta), Nile Red was used for lipid droplets (red), and Hoechst counterstaining was used to visualize nuclei (blue) of fibrin only drops incubated in brown adipogenic differentiation medium (BAM) growth medium (GM) and white adipogenic differentiation medium (WAM) on day 14. UCP1, lipids and nuclei of cells are shown in Merge image (Scale bar: 200 μm). F) Higher magnification of UCP1, lipids and nuclei of cells are shown in Merge image of fibrin only samples in BAM (Scale bar: 50 μm). G) Relative gene expressions of several brown adipogenic markers on day 14. Uncoupling protein 1 (UCP1), cell death-inducing DNA fragmentation factor alpha-like effector A (Cidea) and PR domain containing 16 (PRDM16). Results are shown as mean ± standard deviation (n = 3, three independent experiments from one donor). Data was normalized by RPII (RNA Polymerase II) the house keeping gene. Statistical differences were obtained by student t-test were shown as * = $p < 0.05$, ** = $p < 0.01$. White dots represent data points of each parallel.

adipogenic differentiated and undifferentiated samples cultured in BAM, GM, and WAM respectively, as shown in Fig. 2E. Distinct expressions of both UCP1 and lipid droplet accumulations were exclusively observed in the BAM group. This result confirms the successful occurrence of brown adipogenic differentiation. Accordingly, although the WAM cultured droplets showed lipid accumulation, they were negative for UCP1 expression as expected. In general, white adipocytes do not show UCP1 protein expression [39,40]. In Fig. 2F, higher magnification representation of samples cultured in BAM is shown. The relative gene expression levels of BAT-specific genes, UCP1, Cidea, and PRDM16, were finally assessed by the RT-qPCR analyses. UCP1 serves as a primary thermogenic marker and plays a crucial role in fatty acid metabolism [41]. The outcomes showed expressions of these brown

adipogenic-related genes were markedly elevated in comparison to undifferentiated cells cultured in GM (Fig. 2G). Specifically, the gene expressions of UCP1, Cidea, and PRDM16 were determined to be 58 (±16), 198 (±71), and 4.7 (±0.8) times higher, respectively, in the BAM groups compared to the GM counterparts. This significant difference observed in brown-specific genes further corroborates the process of browning. Based on the comprehensive findings obtained from the evaluation of various parameters, it is substantiated that the BAM exerts a notable impact on DFATs encapsulated in fibrin gel and cultured for a duration of 14 days in terms of browning. This efficacy is evident across multiple aspects, including lipid droplet size measurements, mitochondrial abundance assessments, immunocytochemical analyses of UCP1, and BAT markers' gene expression evaluations. This culture medium and the

fibrin gel culture conditions were thus used for the next steps assessing the effect of various added polymers.

4.2. UCP1 and lipid contents of polymer-mixed samples

PLL is well known for its possible cytotoxic effect [42]. Therefore, before mixing it in the fibrin gel tissues, different concentrations were compared. The other polymers were added at a final concentration of 50 µg/mL, following the protocol in our previous study [26]. PLL was used at a concentration of 10 µg/mL based on cell viability analysis results (Supplementary Fig. 1), since viability was observed to be only 26 % (±6) in drops containing 50 µg/mL PLL, while all other concentrations exhibited viabilities exceeding 80 %. Additionally, DNA quantification analysis (Supplementary Fig. 2) revealed that drops containing 10 µg/mL PLL exhibited a similar amount of DNA content to fibrin-only drops by the 14th day (174 ± 27 ng/mL for fibrin only, 174 ± 55 ng/mL for PLL group). Since the amount of RNA in cells can serve as a valuable indicator of cell viability, the RNA concentrations measured

after RNA extraction were examined. It was found that the droplets containing 5 µg/mL PLL had 63 (±3) ng/mL RNA, while the droplets containing 10 and 20 µg/mL PLL had RNA concentrations of 37 (±4) and 33 (±10) ng/mL, respectively. However, DNA quantification analysis and live/dead staining showed that 10 µg/mL PLL is acceptable in terms of cell viability. Based on these findings, it was decided to maintain the PLL concentration at 10 µg/mL for subsequent experiments related to browning.

UCP1 immunofluorescence staining of the polymer-mixed samples (Fig. 3A) was then assessed and all confirmed the brown adipogenic differentiation of DFATs in fibrin-only and polymer-mixed fibrin gel on day 14 in the BAM condition. Additionally, the high magnification images of PLL-mixed droplets, and the separate channel images of nuclei, lipid, and UCP1 content are shown in Supplementary Fig. 5.

For the quantification of UCP1 and lipid content in the samples, the fluorescence intensity of each drop was normalized by DNA fluorescence (Fig. 3B, white bars). Analyses revealed that none of the polymers, except PLL, tended to induce an increase in UCP1 content (white bars).
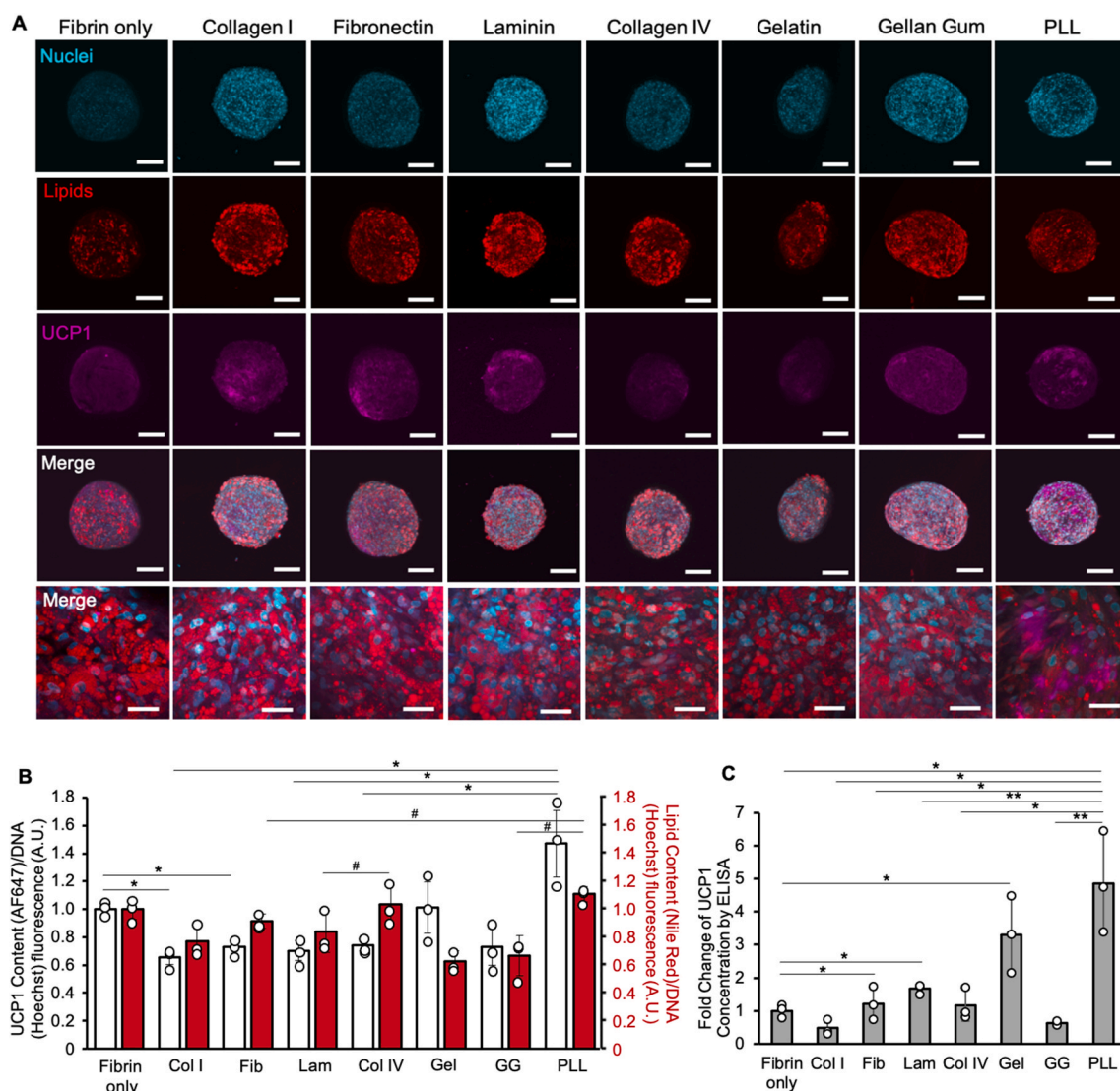

Fig. 3. A) Representative images of immunocytochemical staining of UCP1 (magenta), lipid droplets by Nile Red (red), and Hoechst counterstaining was used to visualize nuclei (blue) of polymer mixed brown-like adipose drops on day 14. UCP1, lipids and nuclei of cells are shown in Merge image (Scale bar: 200 µm, for high magnification image scale bar: 50 µm). B) Measurements of the UCP1 (light grey bars) and Nile Red fluorescence of drops (red bars), normalized by either the DNA (Hoechst) fluorescence. Results are shown as mean ± standard deviation (n = 3, three independent samples from one donor). Statistical differences were obtained by Anova statistical tests were shown as * = $p < 0.05$ for UCP1, # = $p < 0.05$ for lipids. C) UCP1 Elisa results of polymer mixed drops. Results are shown as mean ± standard error (n = 3, three independent experiments from one donor). Statistical differences were obtained by Anova statistical tests were shown as * = $p < 0.05$. White dots represent data points of each parallel.

In drops containing PLL, the fluorescence intensity of UCP1 was 1.5 times higher ($\pm$0.2) compared to the fibrin-only group, although it was not statistically significant ($p > 0.0509$). In a comparable manner, the measured lipid content revealed that no statistically significant difference was observed among polymer-mixed groups when compared exclusively to samples containing only fibrin (Fig. 3B, red bars). However, statistically significant differences were evident between laminin and collagen type IV, as well as PLL and GG and fibronectin groups. Remarkably, PLL exhibited the highest lipid content value in this statistical comparison of 1.1 ($\pm$0.1). Immunofluorescent images indicate that PLL may have increased both UCP1 expression and lipid content. The UCP1 concentrations in polymer-mixed samples were confirmed by ELISA assay and compared with those from the fibrin-only group (Fig. 3C), normalized by DNA content. Notably, PLL demonstrated the highest relative concentration of 5 ($\pm$2), compared to the fibrin only group, while an increase in UCP1 concentration was also observed in the case of gelatin, laminin, and fibronectin mixed drops albeit to a lesser extent. This ELISA result further supports the inducing effect of PLL on brown adipogenesis.

4.3. Relative gene expression analysis of polymer-mixed brown-like drops

The relative gene expression of the three brown adipogenic markers UCP1, Cidea and PRDM16 was next analyzed to confirm the brown adipogenic differentiation of DFATs in fibrin-only and polymer-mixed fibrin gels (Fig. 4). PLL-mixed drops (10 μg/mL), when compared to the other groups, induced a significantly higher UCP1 gene expression, with a relative fold increase value of 6 ($\pm$3) compared to fibrin only. Additionally, an increase in PLL concentration in PLL-mixed droplets, with fibrin gel, at concentrations of 5, 10, and 20 μg/mL resulted in a corresponding increase in UCP1 expression, with values from 1 ($\pm$0.3) to 2.07 ($\pm$0.01) (Fig. 4A, right graph), further confirming the meaningful effect of PLL on the brown adipogenesis differentiation induction. Concerning the Cidea gene (Fig. 4B), samples containing PLL (10 μg/mL) had the highest expression at 3 ($\pm$3). However, the PLL concentration effect on Cidea relative gene expression was not significant, with a
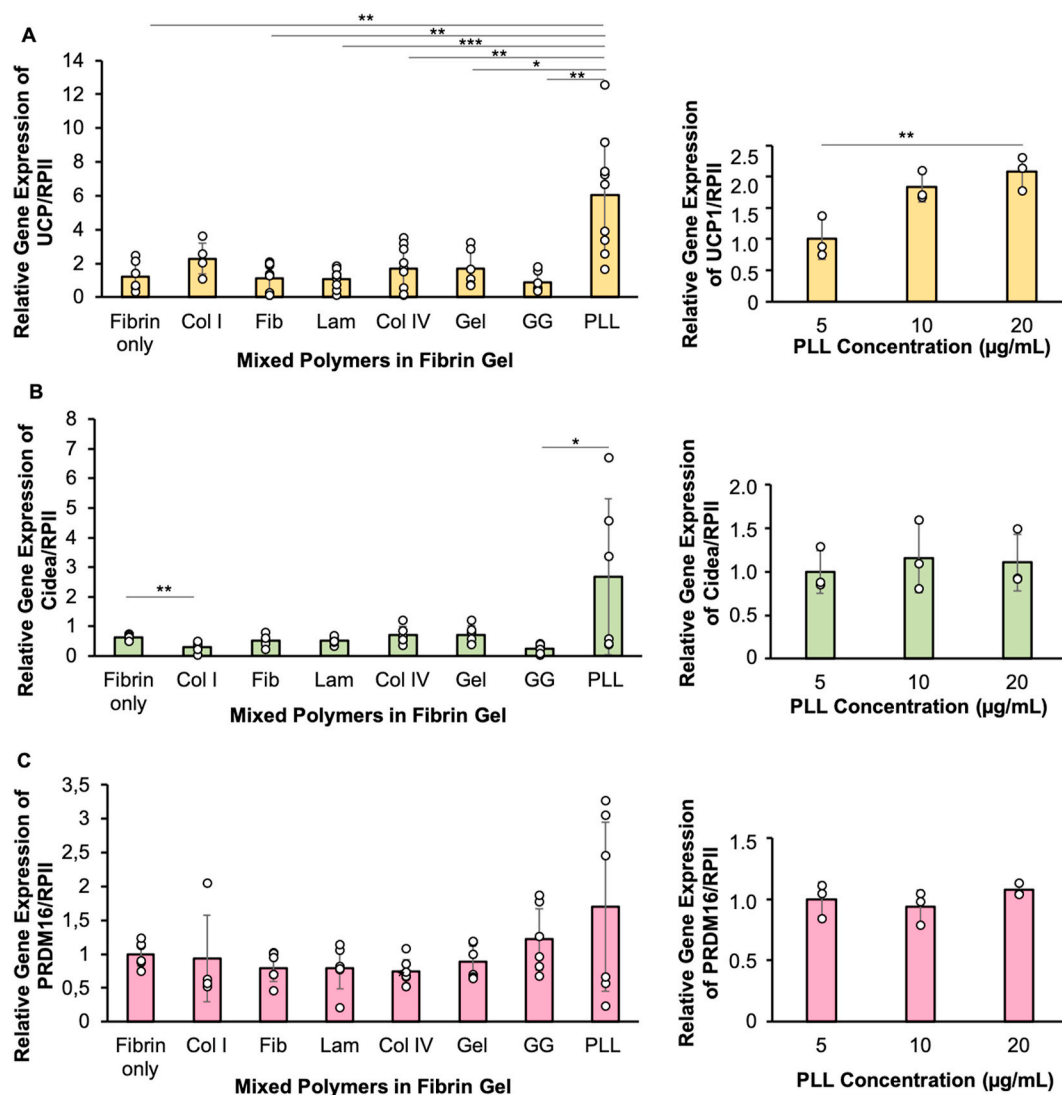

Fig. 4. Relative gene expressions of several brown adipogenic markers. A) Uncoupling protein 1 (UCP1), results are shown as mean $\pm$ standard error. The results shown as means $\pm$ s.d. of experiments performed on N = 4–9, using 3 different patients' cells for left graph, n = 3 using 1 patient's cells for right graph. * = $p < 0.05$, ** = $p < 0.01$, *** = $p < 0.001$. B) Cell death-inducing DNA fragmentation factor alpha-like effector A (Cidea), the results shown as means $\pm$ s.d. of experiments performed on N = 4–6, using 2 different patients' cells for left graph, n = 3 using 1 patient's cells for right graph. * = $p < 0.05$, ** = $p < 0.01$. C) PR domain containing 16 (PRDM16). The results shown as means $\pm$ s.d. of experiments performed on N = 4–6, using 2 different patients' cells for left graph, n = 3 using 1 patient's cells for right graph. * = $p < 0.05$. PLL was used 10 μg/mL for left graph. Statistical differences were obtained by student-t tests were shown as * = $p < 0.05$. White dots represent data points of each parallel.

maximum of 1.1 (±0.3) for 20 µg/mL. Finally, for PRDM16 relative gene expression, the results were not significantly different but a similar trend could be observed in samples containing PLL (10 µg/mL), mirroring the UCP1 and Cidea gene expression values. For the PLL concentration

comparison, as for Cidea, no significant difference was evident, the relative expression being 1.07 (±0.05) for 20 µg/mL. In terms of browning, PLL exhibited an increasing trend in the expression of brown-specific genes. However, the increased concentration of PLL did not
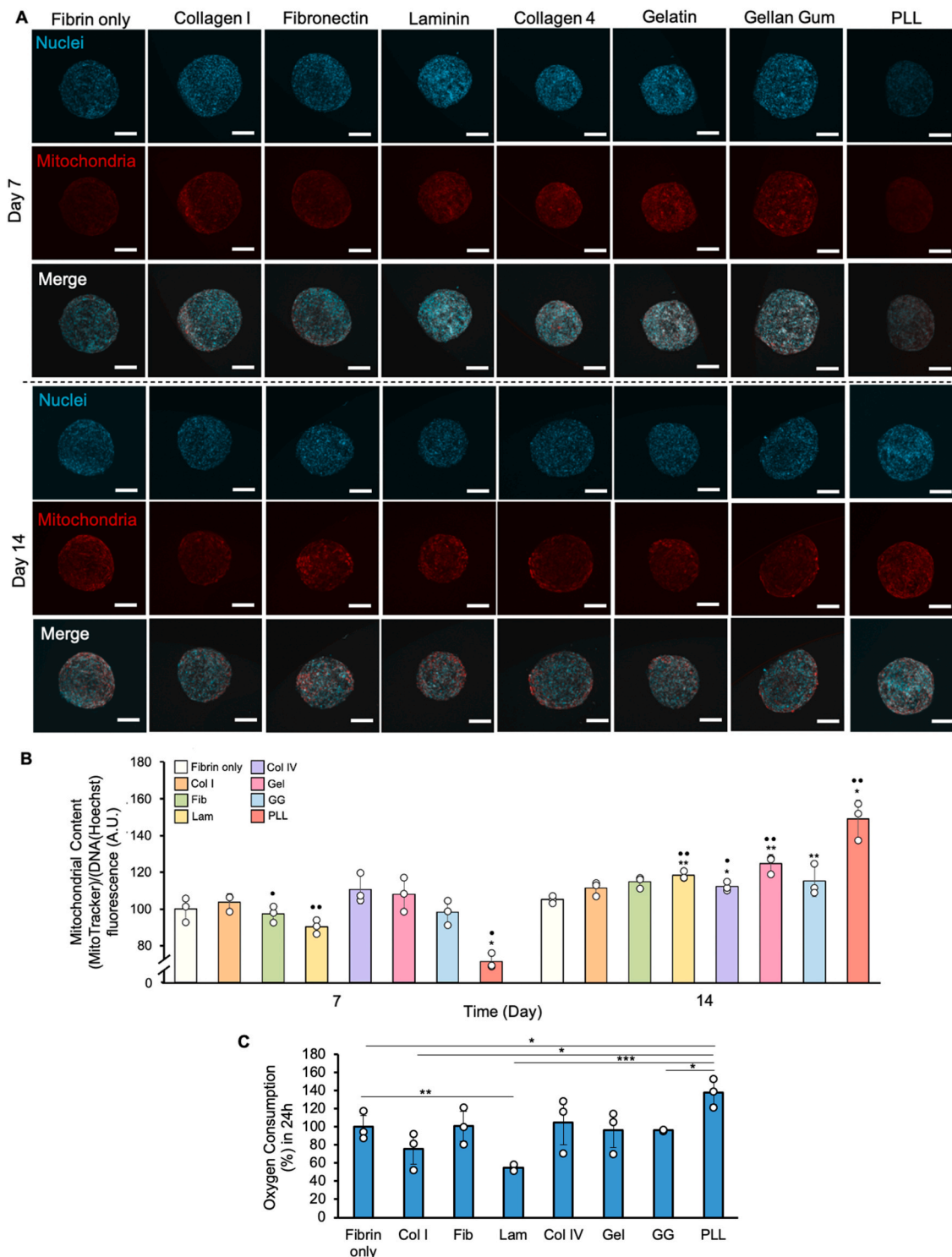

Fig. 5. Representative MitoTracker staining images of mitochondria (red) and Hoechst counterstaining was used to visualize nuclei (blue) drops incubated in BAM on day 7 and 14. The mitochondria and nuclei of cells are shown in Merge image (Scale bar: 200 µm) B) The measurement of the MitoTracker fluorescence of the samples, normalized either the DNA (Hoechst) fluorescence. Results are shown as mean ± standard error (n = 3, three independent experiments from one donor). Statistical differences were obtained by Anova statistical tests were shown as * = $p < 0.05$. * = $p < 0.05$, ** = $p < 0.01$ when compare with day 7 fibrin only group as control. • = $p < 0.05$, •• = $p < 0.01$ when compare with day 14 fibrin only group as control. C) Oxygen consumption percentages in 24 h. Results are shown as mean ± standard error (n = 3, three independent experiments from one donor). Statistical differencies were obtained by Anova statistical tests were shown as * = $p < 0.05$, ** = $p < 0.01$, *** = $p < 0.001$. White dots represent data points.

result in a significant difference, except for UCP1 gene expression ($p <$ 0.01).

4.4. Mitochondrial assessments of polymer-mixed brown-like drops

To further assess the impact of the added polymers on the mitochondrial content during brown adipogenic differentiation, the

mitochondrial abundance of polymer-mixed samples cultured with BAM was evaluated on days 7 and 14 (Fig. 5A) and the quantification was normalized by DNA fluorescence intensity (Fig. 5B). Samples containing only fibrin (on day 7) were compared with polymer-mixed samples at both time points (7th and 14th days) and the fibrin-only group (on day 14). Accordingly, when they were examined on the 7th day, the mitochondrial abundance in drops containing polymers was not higher than
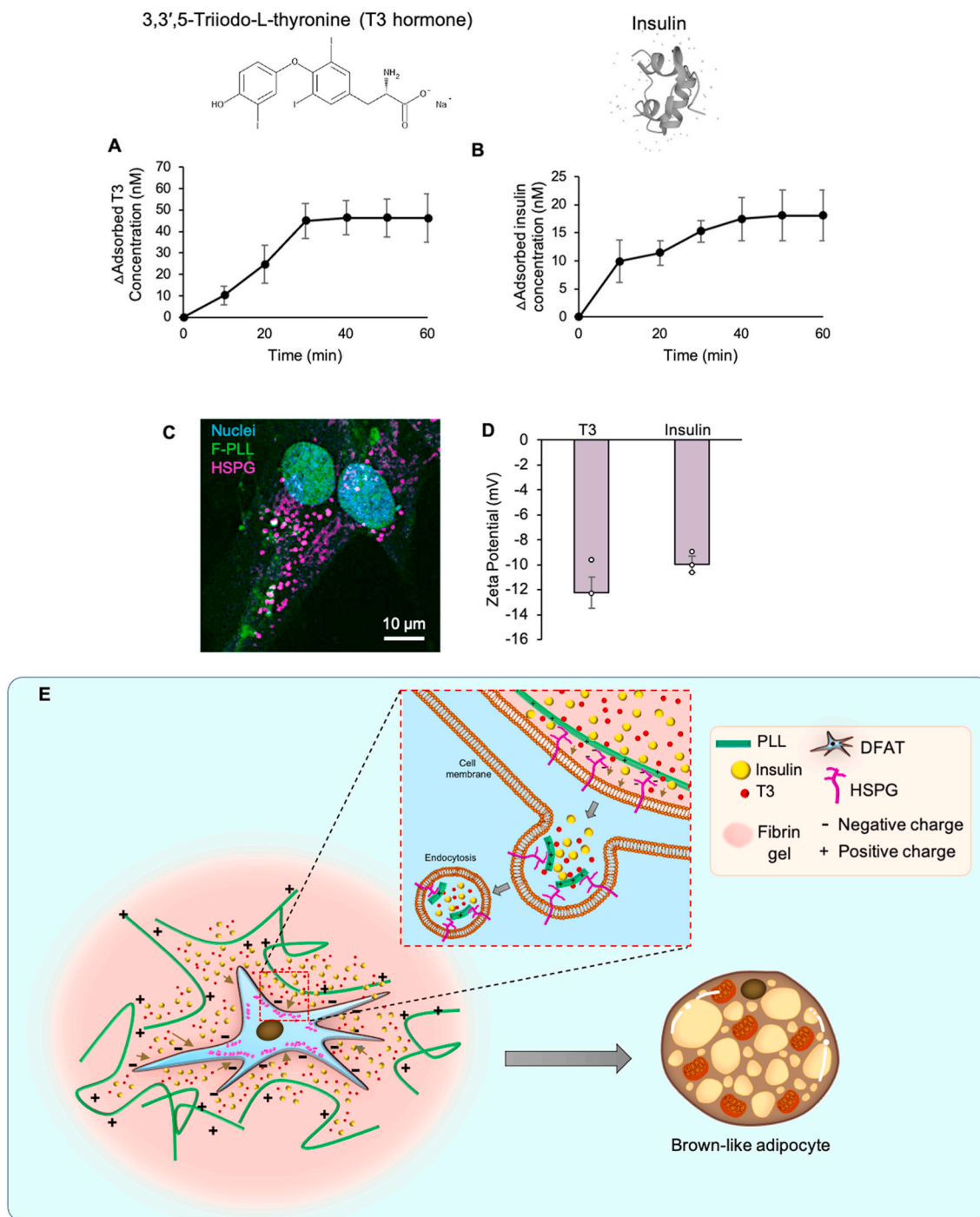

Fig. 6. Conclusion of the study. A) T3 adsorption monitoring on PLL coating surface according to the time duration based on 302 nm absorption point (n = 3, three independent experiments). B) Insulin adsorption monitoring on PLL coating surface according to the time duration based on 277 nm absorption point (n = 3, three independent experiments). C) Representative HSPG staining image of DFATs incubated in GM included F-PLL (green). HSPG (magenta) and Hoechst counterstaining was used to visualize nuclei (blue) (Scale bar: 10 μm). D) Zeta potential of T3 and Insulin solutions (n = 3, three independent experiments). E) Expected redifferentiation mechanism of DFATs into brown-like adipocyte in PLL mixed fibrin gel. Positively charged PLL may increase the cellular intake of T3 and insulin during brown adipogenic induction.

that in the fibrin-only group. While the PLL-containing drops exhibited significantly lower mitochondrial content on the 7th day, a surprising increase was observed by the 14th day, reaching 163 ($\pm$11) compared to the day 7 fibrin only samples (100 $\pm$ 7). Moreover, across all groups, an increase in mitochondrial quantity over time was observed, and this increase was statistically significant for laminin, collagen type IV, and GG drops compared with fibrin only drops. The increasing abundance of mitochondria throughout the culture period may suggest that cells continue their brown adipogenic differentiation. The measurement of basal oxygen consumption rates in adipocytes has also been previously reported in the literature [43]. Accordingly, the oxygen consumption rate of the samples was assessed on the 14th day and the oxygen consumption rate over a 24-h period from this day was calculated (Fig. 5C). As a result, the oxygen consumption rate within 24 h was highest in drops containing PLL, reaching a significantly greater value of 138 ($\pm$13) than fibrin only drops (100 $\pm$ 13). However, in collagen type I and laminin drops, oxygen consumption decreased, while the remaining groups exhibited values close to the fibrin-only group. These data further confirm PLL's inducing effect on brown adipogenesis and increases in metabolic activity.

4.5. PLL integration on the DFATs

To confirm the interaction between PLL and DFAT, DFATs were incubated for 24 h in culture medium containing FITC-labeled PLL (green, Fig. 6C). Additionally, as PLL is known to possibly interact on heparan sulphate proteoglycans (HSPG), the location of HSPG was also identified by immunostaining. As seen in Fig. 6C, an association between the positively charged polymer and the expression of negatively charged HSPG (magenta) could be identified on the immunofluorescent images that might explain how PLL can bind to the cell surface. In Fig. 6E, the potential mechanism of PLL integration and the subsequent increase in brown adipogenic inducing molecules are illustrated.

4.6. Monitoring T3 and insulin adsorption on PLL coated surfaces

Positively charged PLL can also interact with negatively charged proteins, especially culture medium components. PLL might thus promote the adsorption of specific hormones or proteins from the culture medium that play a role in brown adipocyte differentiation induction. To test this hypothesis and further explain the PLL effect for cell browning, T3 and insulin components of the BAM were chosen. Time-dependent adsorption curves of T3 and insulin on PLL-coated surface were observed (Fig. 6A and B), by using the UV absorbance spectra of T3 and insulin (Supplementary Fig. 3). T3 exhibited a peak at around 240–300 nm wavelength and significantly accumulated on the surface after approximately 30 min ($p < 0.05$). Insulin, on the other hand, peaked in the wavelength range of 240–285 nm and reached a maximum adsorption on the surface after around 50 min ($p < 0.05$). Finally, to validate that this adsorption is related to charge interactions, the zeta potentials of T3 and insulin (-12 ± 1 and -10 ± 0.7 mV, respectively) were assessed (Fig. 6D). Their confirmed negative charges may cause the observed accumulation due to the electrostatic interaction with PLL. These results indicate that PLL may interact with insulin and T3 with electrostatic interaction subsequently enhancing their cellular bioavailability for the DFAT leading to an increased browning differentiation.

5. Discussion

In this study, we evaluated the impact of various polymers mixed into a fibrin matrix on browning. As expected, we first confirmed the brown adipogenic differentiation effect of BAM on DFAT encapsulated in fibrin gel. While examining the effect of the medium initially, we conducted various comparisons, taking into consideration factors such as the lipid droplet size and metabolic differences such as mitochondrial

abundance and oxygen consumption rate. As clearly identified, the morphology of lipid droplets in brown and white adipocytes demonstrates notable differences, with intracellular lipid droplets appearing large and uniocular in WAT and small and multilocular in BAT [44–46]. As illustrated in Fig. 2A and B, the lipid droplet diameters of brown-like adipocytes were confirmed to be significantly smaller that their white differentiated counterparts. Indeed, the unique lipid accumulation patterns in adipocytes actually reflect the functional properties of the fat cells. White adipocytes efficiently store triacylglycerol in large lipid droplets, while brown adipocytes store lipids in small, multilocular ones that facilitate the transport of free fatty acids to mitochondria, promoting effective lipolysis and heat production [44]. On the other hand, it is known that the increased mitochondrial activity and abundance in brown adipocytes are associated with their non-shivering thermogenesis ability [47]. The pivotal factor responsible for this unique process is UCP1, a protein that briefly allows for the generation of heat instead of ATP by increasing the permeability of the inner mitochondrial membrane in BAT mitochondria [48,49]. In Fig. 2C and D, when compared with undifferentiated cells cultured in GM, the increased mitochondrial content in brown-differentiated cells served as evidence confirming the successful occurrence of brown adipogenic differentiation, in addition to the confirmed presence of UCP1 by immunocytochemical staining (Fig. 2E). The increased expressions of brown-related mRNA expressions was also observed as shown in Fig. 2G. Here, alongside the validation of UCP1 gene expression, the increased expression of two other brown-related mRNAs which are Cidea (involved in lipid droplet remodeling [41,44]) and PRDM16 (involved in controlling the differentiation-linked brown fat gene program [41,50]) has confirmed the process of brown adipogenesis. In the subsequent step, we aimed to assess the impact of various polymers on browning. While the mechanism of how local factors influence stem cell fate is highly complex, polymers, as the external factors, can indeed affect crucial cellular processes such as differentiation, proliferation or apoptosis [51]. Moreover, in combination with all these factors, the process of adipocyte differentiation is complex, demanding coordinated communication between external stimuli within a network of receptors and transcription factors in the nucleus [52]. Consequently, few studies exist on the effect of polymers on stem cell adipogenesis signaling, especially for browning induction. On one hand, regarding the effect of ECM-related polymers, Porras et al. demonstrated that mouse ADSCs cultured in an environment inducing browning on surfaces coated with collagen type I and laminin exhibited a decreased tendency for differentiation into brown-like adipocytes. They suggested that the ECM molecules found at higher levels in WAT may lead to a decrease in thermogenic capacity by inhibiting UCP1 expression [53]. In our findings, as demonstrated in Figs. 3–5, the drops mixed with ECM molecules supported the reported results, indicating lower UCP1 expressions and a relatively lower oxygen consumption rate. However, in another related study [31], human MSCs and endothelial cells were co-encapsulated in a collagen type I gel and cultured in a BAM. The system demonstrated inducibility for brown adipogenesis, shown by increased PGC1-α and UCP1 mRNA expression in differentiating stem cells. The importance of endothelial-stem cell crosstalk for brown adipogenesis was also emphasized and within the collagen type I gel, the 1:1 co-culture displayed the most comprehensive vascular network formation, suggesting a supportive environment for vascular network development and supporting the upregulation of vascular endothelial growth factor which can be supporting for brown adipogenesis [31]. On the other hand, while the impact of charged polymers on adipogenic differentiation is a promising topic, there are intriguing findings in the literature, particularly focusing on *in vitro* white adipogenesis. The addition of metal ions (Cu^{2+}, Fe^{3+}) to polyelectrolyte multilayers (PEMs) made from chitosan and alginate can promote cell adhesion and adipogenic differentiation on stem cells and fibroblasts. The specific mechanisms by which metal ions influence adipogenesis may not be fully understood but it has been indicated that these ions assist in better cell adhesion and the initiation of adipocyte

differentiation by binding to the polysaccharide layers [54,55]. In another study, photoreactive polyelectrolytes such as polyallylamine (PAAm) and poly (acrylic acid) (PAAc) have been demonstrated to support the adipogenesis of MSCs. These modified surfaces can facilitate cell attachment and adhesion, thereby promoting adipogenic differentiation [56]. Lee et al. showed that PLL can enhance the white adipogenic differentiation of both 3T3-L1 preadipocytes and hMSC by activating the insulin signaling pathway. As a possible explanation, they indicated that PLL has the potential to serve as a substitute for insulin, a critical adipogenic inducer [57]. In our study we used brown adipogenic differentiation medium which includes T3 that important brown adipogenic inducer. T3 affects brown adipocyte thermogenesis by acutely increasing UCP1 gene expression via a cyclic adenosine monophosphate (cAMP)-mediated pathway [58] Additionally, when insulin combined with T3 in the differentiation medium, it affects brown adipogenic differentiation by influencing relevant signaling pathways, such as the adenosine 5′-monophosphate (AMP)-activated protein kinase (AMPK) pathway [59]. However, none of these studies evaluated the impact of charged polymers on brown adipogenic differentiation. In the current study, we observed that the cationic polymer PLL can significantly induce brown adipogenic differentiation compared to drops obtained by mixing collagen type I, laminin, fibronectin, collagen type IV, and GG with fibrin gel. Together with immunocytochemical analysis and ELISA assay showing UCP1 expression (Fig. 3), an increase in the BAT-related gene expressions was highlighted in drops containing PLL (Fig. 4). Subsequent mitochondrial analyses, particularly on the 14th day, further confirmed the significant increase in both mitochondrial quantity and oxygen consumption rate due to PLL (Fig. 5). One possible reason for the high error bars observed in Fig. 4 could be the age-related decrease in the cellular differentiation abilities of DFATs obtained from adipose tissues from different donors. Increased donor age has been reported to negatively impact the differentiation abilities of stem cells in various studies [60,61]. Therefore, cells obtained from donors with ages ranging from 41 to 53 may be the cause of the high standard deviations. On the other hand, while the increased PLL concentration only leads to a significant increase in UCP1 gene expression (Fig. 4A, right chart), it can be observed that there is no significant difference between the groups when considering the expressions of Cidea and PRDM16 genes. One possible explanation is the fact that Cidea and PRDM16 are early gene markers compared to UCP1 [62,63], and their expression already decreased leading to UCP1 late marker increase. Moreover, considering the cytotoxicity associated with increasing concentrations of polycations [64], we came to the conclusion that choosing a relatively moderate concentration would be more advantageous in this study. To go into further detail about the possible cellular mechanism of the PLL, a linear lysine polymer carrying a positive charge at neutral pH, it can interact electrostatically with negatively charged molecules on the cell surface. One possibility is its interaction with the negatively charged heparan sulphate proteoglycans (HSPG) as a first step, leading to cell surface HSPGs mediated endocytosis [65]. In Fig. 6C, the interaction between FITC-labeled PLL and cell HSPGs can be observed. Based on these findings, we hypothesized that the enhancing effect of PLL on brown adipogenic differentiation could be attributed to the co-internalization of insulin, an effective agent for both white and brown adipogenic differentiation, and the thyroid hormone T3, a crucial factor in brown adipogenic differentiation. Numerous *in vitro* studies on brown adipogenic differentiation involve the inclusion of T3 in the brown adipogenic differentiation cocktail [61]. T3 hormone activates thermogenesis by uncoupling electron transfer in BAT mitochondria from ATP synthesis. Consequently, it is also an important regulator of basal metabolic rate, and therefore, hypothyroid patients often clinically manifest as overweight [66]. It also influences brown adipocyte thermogenesis by increasing the stimulatory effect of norepinephrine (NE) and enhancing the acute elevation of cAMP-mediated UCP1 gene expression [67]. In light of this information, considering the zeta potential of the T3 and the insulin (Fig. 6D), their electrostatic interactions with the positively

charged PLL provide a possible hypothesis as summarized in Fig. 6E. Therefore, by initially interacting with the negatively charged HSPG on the cell surface, PLL may facilitate the uptake of both T3 and insulin into the cells, thereby triggering brown adipogenesis. However, it is difficult to predict whether the observed effects are due to the impact of PLL on the differentiation process itself or due to the effect of PLL-mediated added hormones [68].

6. Conclusion

In conclusion, our study explored the impact of the culture medium and various polymers integrated into the fibrin matrix on the process of brown adipogenic differentiation. In particular, our findings indicated that the incorporation of the cationic polymer PLL into the fibrin gel can significantly increase brown adipogenesis, leading to distinct inductions in the differentiation mechanism compared to other polymers. The observed electrostatic interaction between PLL and HSPG on the cell surface suggested a potential mechanism for PLL in facilitating the uptake of insulin and T3, thereby contributing to brown adipogenic differentiation. Our results shed light on the complex interplay of factors influencing brown adipogenesis, highlighting PLL as a promising candidate for inducing this intricate process. We believe that further research is essential to delve into these intricate molecular mechanisms to uncover potential applications for cationic polymers in the realm of brown adipogenic differentiation. We further hope that our research will contribute materially to future studies in this field.

CRediT authorship contribution statement

Aslı Sena Karanfil: Writing – review & editing, Writing – original draft, Visualization, Validation, Methodology, Investigation, Conceptualization. **Fiona Louis:** Writing – review & editing, Validation, Supervision, Project administration, Data curation, Conceptualization. **Yoshihiro Sowa:** Supervision, Resources. **Michiya Matsusaki:** Supervision, Resources, Project administration, Methodology, Funding acquisition.

Declaration of competing interest

The authors declare that they have no known competing financial interests or personal relationships that could have appeared to influence the work reported in this paper.

Data availability

Data will be made available on request.

Acknowledgments

Appendix A. Supplementary data

Supplementary data to this article can be found online at https://doi.org/10.1016/j.mtbio.2024.101157.

References

[1] A. Armani, C. Mammi, V. Marzolla, M. Calanchini, A. Antelmi, G.M.C. Rosano, A. Fabbri, M. Caprio, Cellular models for understanding adipogenesis, adipose dysfunction, and obesity, J. Cell. Biochem. 110 (2010), https://doi.org/10.1002/jcb.22598.

[2] T. Scully, A. Ettela, D. LeRoith, E.J. Gallagher, Obesity, type 2 diabetes, and cancer risk, Front. Oncol. 10 (2021), https://doi.org/10.3389/fonc.2020.615375.

[3] A.O. Silva, M.V. Silva, L.K.N. Pereira, W.M.N. Feitosa, R.M. Ritti-Dias, P.R.B. Diniz, L.M.F.T. Oliveira, Association between general and abdominal obesity with high blood pressure: difference between genders, J. Pediatr. 92 (2016), https://doi.org/10.1016/j.jped.2015.05.007.

[4] Š. Svačina, Obesity and cardiovascular disease, Vnitr. Lek. 66 (2020), https://doi.org/10.1161/01.atv.0000216787.85457.f3.

[5] D. Antillon, A. Towfighi, No time to "weight": the link between obesity and stroke in women, Wom. Health 7 (2011), https://doi.org/10.2217/whe.11.36.

[6] H. Lee, Obesity-associated cancers: evidence from studies in mouse models, Cells 11 (2022), https://doi.org/10.3390/cells11091472.

[7] E.W. Edmonds, K.J. Templeton, Childhood obesity and musculoskeletal problems: editorial comment, Clin. Orthop. Relat. Res. 471 (2013), https://doi.org/10.1007/s11999-013-2815-z.

[8] D.A. Fitzgerald, The weighty issue of obesity in paediatric respiratory medicine, Paediatr. Respir. Rev. 24 (2017), https://doi.org/10.1016/j.prrv.2017.06.008.

[9] T. Lobstein, R. Jackson-Leach, J. Powis, H. Brinsden, M. Gray, World Obesity Atlas 2023, World Obesity Federation, 2023.

[10] A. Smorlesi, A. Frontini, A. Giordano, S. Cinti, The adipose organ: white-brown adipocyte plasticity and metabolic inflammation, Obes. Rev. 13 (2012) 83–96, https://doi.org/10.1111/j.1467-789X.2012.01039.x.

[11] J. Wu, P. Boström, L.M. Sparks, L. Ye, J.H. Choi, A.H. Giang, M. Khandekar, K. A. Virtanen, P. Nuutila, G. Schaart, K. Huang, H. Tu, W.D. Van Marken Lichtenbelt, J. Hoeks, S. Enerbäck, P. Schrauwen, B.M. Spiegelman, Beige adipocytes are a distinct type of thermogenic fat cell in mouse and human, Cell 150 (2012) 366–376, https://doi.org/10.1016/j.cell.2012.05.016.

[12] S. Cinti, Pink adipocytes, Trends Endocrinol. Metabol. 29 (2018) 651–666, https://doi.org/10.1016/j.tem.2018.05.007.

[13] J.C. George, J. Eapen, A histological and histochemical study of the Brown and yellow adipose tissue of the bat, hipposideros speoris, J. Cell Sci. S3–100 (1959), https://doi.org/10.1242/jcs.s3-100.51.369.

[14] A.S. Karanfil, F. Louis, M. Matsusaki, Biofabrication of vascularized adipose tissues and their biomedical applications, Mater. Horiz. 10 (2023), https://doi.org/10.1039/d2mh01391f.

[15] D.F. Pisani, V. Barquissau, J.C. Chambard, D. Beuzelin, R.A. Ghandour, M. Giroud, A. Mairal, S. Pagnotta, S. Cinti, D. Langin, E.Z. Amri, Mitochondrial fission is associated with UCP1 activity in human brite/beige adipocytes, Mol. Metabol. 7 (2018), https://doi.org/10.1016/j.molmet.2017.11.007.

[16] E.T. Chouchani, L. Kazak, B.M. Spiegelman, New advances in adaptive thermogenesis: UCP1 and beyond, Cell Metabol. 29 (2019), https://doi.org/10.1016/j.cmet.2018.11.002.

[17] M. Christian, In vitro models for study of brown adipocyte biology, Handb. Exp. Pharmacol. 251 (2019) 85–96, https://doi.org/10.1007/164_2018_122.

[18] M. Jumabay, Dedifferentiated fat cells: a cell source for regenerative medicine, World J. Stem Cell. 7 (2015), https://doi.org/10.4252/wjsc.v7.i10.1202.

[19] H. Sugihara, N. Yonemitsu, S. Miyabara, K. Yun, Primary cultures of unilocular fat cells: characteristics of growth in vitro and changes in differentiation properties, Differentiation 31 (1986), https://doi.org/10.1111/j.1432-0436.1986.tb00381.x.

[20] J.E. Watson, N.A. Patel, G. Carter, A. Moor, R. Patel, T. Ghansah, A. Mathur, M. M. Murr, P. Bickford, L.J. Gould, D.R. Cooper, Comparison of markers and functional attributes of human adipose-derived stem cells and dedifferentiated adipocyte cells from subcutaneous fat of an obese diabetic donor, Adv. Wound Care 3 (2014) 219–228, https://doi.org/10.1089/wound.2013.0452.

[21] T. Yanagi, H. Kajiya, S. Fujisaki, M. Maeshiba, A. Yanagi-S, N. Yamamoto-M, K. Kakura, H. Kido, J. Ohno, Three-dimensional spheroids of dedifferentiated fat cells enhance bone regeneration, Regen Ther 18 (2021), https://doi.org/10.1016/j.reth.2021.10.004.

[22] T. Kazama, M. Fujie, T. Endo, K. Kano, Mature adipocyte-derived dedifferentiated fat cells can transdifferentiate into skeletal myocytes in vitro, Biochem. Biophys. Res. Commun. 377 (2008), https://doi.org/10.1016/j.bbrc.2008.10.046.

[23] M. Shimizu, T. Matsumoto, S. Kikuta, M. Ohtaki, K. Kano, H. Taniguchi, S. Saito, M. Nagaoka, Y. Tokuhashi, Transplantation of dedifferentiated fat cell-derived micromass pellets contributed to cartilage repair in the rat osteochondral defect model, J. Orthop. Sci. 23 (2018), https://doi.org/10.1016/j.jos.2018.03.001.

[24] X. Hu, P. Luo, X. Peng, T. Song, Y. Zhou, H. Wei, J. Peng, S. Jiang, Molecular cloning, expression pattern analysis of porcine Rb1 gene and its regulatory roles during primary predifferentiation fat cells adipogenic differentiation, Gen. Comp. Endocrinol. 214 (2015), https://doi.org/10.1016/j.ygcen.2015.01.016.

[25] J. Lessard, J.A. Côté, M. Lapointe, M. Pelletier, M. Nadeau, S. Marceau, L. Biertho, A. Tchernof, Generation of human adipose stem cells through dedifferentiation of mature adipocytes in ceiling cultures, JoVE 2015 (2015), https://doi.org/10.3791/52485.

[26] A.S. Karanfil, F. Louis, Y. Sowa, M. Matsusaki, ECM proteins and cationic polymers coating promote dedifferentiation of patient-derived mature adipocytes to stem cells, Biomater. Sci. 11 (2023) 7623–7638, https://doi.org/10.1039/d3bm00934c.

[27] M.C. Tanzi, S. Farè, Adipose tissue engineering: state of the art, recent advances and innovative approaches, Expet Rev. Med. Dev. 6 (2009) 533–551, https://doi.org/10.1586/erd.09.37.

[28] C.S. Murphy, L. Liaw, M.R. Reagan, In vitro tissue-engineered adipose constructs for modeling disease, BMC Biomed. Eng 1 (2019) 1–19, https://doi.org/10.1186/s42490-019-0027-7.

[29] K. Hemmrich, D. von Heimburg, Biomaterials for adipose tissue engineering, Expet Rev. Med. Dev. 3 (2006) 635–645, https://doi.org/10.1586/17434440.3.5.635.

[30] K.M. Tharp, A. Stahl, Bioengineering beige adipose tissue therapeutics, Front. Endocrinol. 6 (2015) 1–9, https://doi.org/10.3389/fendo.2015.00164.

[31] J.H. Hammel, E. Bellas, Endothelial cell crosstalk improves browning but hinders white adipocyte maturation in 3D engineered adipose tissue, Integr. Biol. 12 (2020) 81–89, https://doi.org/10.1093/intbio/zyaa006.

[32] K.M. Tharp, A.K. Jha, J. Kraiczy, A. Yesian, G. Karateev, R. Sinisi, E. A. Dubikovskaya, K.E. Healy, A. Stahl, Matrix-assisted transplantation of functional beige adipose tissue, Diabetes 64 (2015) 3713–3724, https://doi.org/10.2337/db15-0728.

[33] M. Kuss, J. Kim, D. Qi, S. Wu, Y. Lei, S. Chung, B. Duan, Effects of tunable, 3D-bioprinted hydrogels on human brown adipocyte behavior and metabolic function, Acta Biomater. 71 (2018) 486–495, https://doi.org/10.1016/j.actbio.2018.03.021.

[34] J.P. Yang, A.E. Anderson, A. McCartney, X. Ory, G. Ma, E. Pappalardo, J. Bader, J. H. Elisseeff, Metabolically active three-dimensional Brown adipose tissue engineered from white adipose-derived stem cells, Tissue Eng. 23 (2017) 253–262, https://doi.org/10.1089/ten.tea.2016.0399.

[35] M.K. Vaicik, M. Morse, A. Blagajcevic, J. Rios, J.C. Larson, F. Yang, R.N. Cohen, G. Papavasiliou, E.M. Brey, Hydrogel-based engineering of beige adipose tissue, J. Mater. Chem. B 3 (2015) 7903–7911, https://doi.org/10.1039/c5tb00952a.

[36] K. Wittmann, S. Dietl, N. Ludwig, O. Berberich, C. Hoefner, T. Blunk, P. Bauer-Kreisel, Engineering vascularized adipose tissue using the stromal-vascular fraction and fibrin hydrogels, Tissue Eng. 21 (2015), https://doi.org/10.1089/ten.tea.2014.0299.

[37] F. Louis, S. Kitano, J.F. Mano, M. Matsusaki, 3D collagen microfibers stimulate the functionality of preadipocytes and maintain the phenotype of mature adipocytes for long term cultures, Acta Biomater. 84 (2019) 194–207, https://doi.org/10.1016/j.actbio.2018.11.048.

[38] D. Weidlich, J. Honecker, C. Boehm, S. Ruschke, D. Junker, A.T. Van, M. R. Makowski, C. Holzapfel, M. Claussnitzer, H. Hauner, D.C. Karampinos, Lipid droplet–size mapping in human adipose tissue using a clinical 3T system, Magn. Reson. Med. 86 (2021), https://doi.org/10.1002/mrm.28755.

[39] E. Nyman, S. Bartesaghi, R. Melin Rydfalk, S. Eng, C. Pollard, P. Gennemark, X. R. Peng, G. Cedersund, Systems biology reveals uncoupling beyond UCP1 in human white fat-derived beige adipocytes, NPJ Syst Biol Appl 3 (2017), https://doi.org/10.1038/s41540-017-0027-y.

[40] A.E. Pollard, L. Martins, P.J. Muckett, S. Khadayate, A. Bornot, M. Clausen, T. Admyre, M. Bjursell, R. Fiadeiro, L. Wilson, C. Whilding, V.N. Kotiadis, M. R. Duchen, D. Sutton, L. Penfold, A. Sardini, M. Bohlooly-Y, D.M. Smith, J.A. Read, M.A. Snowden, A. Woods, D. Carling, AMPK activation protects against diet-induced obesity through Ucp1-independent thermogenesis in subcutaneous white adipose tissue, Nat. Metab. 1 (2019), https://doi.org/10.1038/s42255-019-0036-9.

[41] S.N. Shapira, P. Seale, Transcriptional control of Brown and beige fat development and function, Obesity 27 (2019), https://doi.org/10.1002/oby.22334.

[42] S. Debnath, A. Mukherjee, S. Karan, M. Debnath, T.K. Chatterjee, Induction of apoptosis, anti-proliferation, tumor-angiogenic suppression and down-regulation of Dalton's Ascitic Lymphoma (DAL) induced tumorigenesis by poly-L-lysine: a mechanistic study, Biomed. Pharmacother. 102 (2018), https://doi.org/10.1016/j.biopha.2018.03.076.

[43] Y. Okamatsu-Ogura, K. Fukano, A. Tsubota, A. Uozumi, A. Terao, K. Kimura, M. Saito, Thermogenic ability of uncoupling protein 1 in beige adipocytes in mice, PLoS One 8 (2013), https://doi.org/10.1371/journal.pone.0084229.

[44] Y. Nishimoto, Y. Tamori, CIDE family-mediated unique lipid droplet morphology in white adipose tissue and brown adipose tissue determines the adipocyte energy metabolism, J. Atherosclerosis Thromb. 24 (2017), https://doi.org/10.5551/jat.RV17011.

[45] M.A. Gonzalez Porras, K. Stojkova, F.M. Acosta, C.R. Rathbone, E.M. Brey, Engineering human beige adipose tissue, Front. Bioeng. Biotechnol. 10 (2022), https://doi.org/10.3389/fbioe.2022.906395.

[46] A. Rashnonejad, G. Ercan, C. Gunduz, A. Akdemir, Y.O. Tiftikcioglu, Comparative analysis of human UCB and adipose tissue derived mesenchymal stem cells for their differentiation potential into brown and white adipocytes, Mol. Biol. Rep. 45 (2018) 233–244, https://doi.org/10.1007/s11033-018-4156-1.

[47] J.H. Lee, A. Park, K.J. Oh, S.C. Lee, W.K. Kim, K.H. Bae, The role of adipose tissue mitochondria: regulation of mitochondrial function for the treatment of metabolic diseases, Int. J. Mol. Sci. 20 (2019), https://doi.org/10.3390/ijms20194924.

[48] A. Fedorenko, P.V. Lishko, Y. Kirichok, Mechanism of fatty-acid-dependent UCP1 uncoupling in brown fat mitochondria, Cell 151 (2012), https://doi.org/10.1016/j.cell.2012.09.010.

[49] P. Ježek, M. Jabůrek, R.K. Porter, Uncoupling mechanism and redox regulation of mitochondrial uncoupling protein 1 (UCP1), Biochim. Biophys. Acta Bioenerg. 1860 (2019), https://doi.org/10.1016/j.bbabio.2018.11.007.

[50] S. Maurer, M. Harms, J. Boucher, The colourful versatility of adipocytes: white-to-brown transdifferentiation and its therapeutic potential in humans, FEBS J. 288 (2021), https://doi.org/10.1111/febs.15470.

[51] N. Zhang, D.H. Kohn, Using polymeric materials to control stem cell behavior for tissue regeneration, Birth Defects Res C Embryo Today 96 (2012), https://doi.org/10.1002/bdrc.21003.

[52] J.M. Moreno-Navarrete, J.M. Fernández-Real, Adipocyte differentiation, in: Adipose Tissue Biology, 2012, https://doi.org/10.1007/978-1-4614-0965-6_2.

[53] M.A. Gonzalez Porras, K. Stojkova, M.K. Vaicik, A. Pelowe, A. Goddi, A. Carmona, B. Long, A.A. Qutub, A. Gonzalez, R.N. Cohen, E.M. Brey, Integrins and extracellular matrix proteins modulate adipocyte thermogenic capacity, Sci. Rep. 11 (2021), https://doi.org/10.1038/s41598-021-84828-z.

[54] H. Kindi, C. Willems, M. Zhao, M. Menzel, C.E.H. Schmelzer, M. Herzberg, B. Fuhrmann, G. Gallego-Ferrer, T. Groth, Metal ion doping of alginate-based

surface coatings induces adipogenesis of stem cells, ACS Biomater. Sci. Eng. 8 (2022), https://doi.org/10.1021/acsbiomaterials.2c00444.

[55] H. Kindi, M. Menzel, A. Heilmann, C.E.H. Schmelzer, M. Herzberg, B. Fuhrmann, G. Gallego-Ferrer, T. Groth, Effect of metal ions on the physical properties of multilayers from hyaluronan and chitosan, and the adhesion, growth and adipogenic differentiation of multipotent mouse fibroblasts, Soft Matter 17 (2021), https://doi.org/10.1039/d1sm00405k.

[56] N. Kawazoe, L. Guo, M.J. Wozniak, Y. Imaizumi, T. Tateishi, X. Zhang, G. Chen, Adipogenic differentiation of mesenchymal stem cells on micropatterned polyelectrolyte surfaces, J. Nanosci. Nanotechnol. 9 (2009), https://doi.org/10.1166/jnn.2009.J003.

[57] K.W. Lee, Y.J. An, J. Lee, J.H. Lee, H.S. Yim, α-Poly-l-lysine functions as an adipogenic inducer in 3T3-L1 preadipocytes, Amino Acids 53 (2021), https://doi.org/10.1007/s00726-020-02932-2.

[58] G. Petito, F. Cioffi, N. Magnacca, P. de Lange, R. Senese, A. Lanni, Adipose tissue remodeling in obesity: an overview of the actions of thyroid hormones and their derivatives, Pharmaceuticals 16 (2023), https://doi.org/10.3390/ph16040572.

[59] J. Pan, S. Kothan, A.T. Moe Moe, K. Huang, Dysfunction of insulin-AKT-UCP1 signalling inhibits transdifferentiation of human and mouse white preadipocytes into brown-like adipocytes, Adipocyte 11 (2022), https://doi.org/10.1080/21623945.2022.2062852.

[60] M.S. Choudhery, M. Badowski, A. Muise, J. Pierce, D.T. Harris, Donor age negatively impacts adipose tissue-derived mesenchymal stem cell expansion and differentiation, J. Transl. Med. 12 (2014), https://doi.org/10.1186/1479-5876-12-8.

[61] C.D.S. Horinouchi, M.J. Barisón, A.W. Robert, C. Kuligovski, A.M. Aguiar, B. Dallagiovanna, Influence of donor age on the differentiation and division

capacity of human adipose-derived stem cells, World J. Stem Cell. 12 (2020), https://doi.org/10.4252/wjsc.v12.i12.1640.

[62] M. Calderon-Dominguez, D. Sebastián, R. Fucho, M. Weber, J.F. Mir, E. García-Casarrubios, M.J. Obregón, A. Zorzano, Á.M. Valverde, D. Serra, L. Herrero, Carnitine palmitoyltransferase 1 increases lipolysis, UCP1 protein expression and mitochondrial activity in brown adipocytes, PLoS One 11 (2016), https://doi.org/10.1371/journal.pone.0159399.

[63] S. Carobbio, A.-C. Guenantin, M. Bahri, I. Samuelson, F. Honig, S. Rodriguez-Fdez, K. Long, I. Kamzolas, S. Awad, D. Lukovic, S. Erceg, A. Bassett, S. Mendjan, L. Vallier, B.S. Rosen, D. Chiarugi, A. Vidal-Puig, Unravelling the developmental roadmap towards human brown adipose tissue Running title: cracking the human BAT developmental path, bioRxiv 16 (3) (2020) 641–655.

[64] E. Naumenko, F. Akhatova, E. Rozhina, R. Fakhrullin, Revisiting the cytotoxicity of cationic polyelectrolytes as a principal component in layer-by-layer assembly fabrication, Pharmaceutics 13 (2021), https://doi.org/10.3390/pharmaceutics13081230.

[65] W.X. Siow, Y.T. Chang, M. Babič, Y.C. Lu, D. Horák, Y.H. Ma, Interaction of poly-L-lysine coating and heparan sulfate proteoglycan on magnetic nanoparticle uptake by tumor cells, Int. J. Nanomed. 13 (2018), https://doi.org/10.2147/IJN.S156029.

[66] R.C. Lindsey, S. Mohan, Thyroid hormone acting via TRβ induces expression of browning genes in mouse bone marrow adipose tissue, Endocrine 56 (2017), https://doi.org/10.1007/s12020-017-1265-x.

[67] N. Martínez-Sánchez, J.M. Moreno-Navarrete, C. Contreras, E. Rial-Pensado, J. Fernø, R. Nogueiras, C. Diéguez, J.M. Fernández-Real, M. López, Thyroid hormones induce browning of white fat, J. Endocrinol. 232 (2017), https://doi.org/10.1530/JOE-16-0425.

[68] M.J. Obregon, Thyroid hormone and adipocyte differentiation, Thyroid 18 (2008), https://doi.org/10.1089/thy.2007.0254.